Time-domain Analytical Method for Aeroelastic Analysis of High Aspect Ratio Wing Using Unsteady Indicial Aerodynamics

Zia Ur REHMAN*

*Corresponding author
Center of Excellence in Science and Applied, Technologies, Islamabad, Pakistan,
zia17uet@gmail.com

DOI: 10.13111/2066-8201.2022.14.3.8

Received: 02 June 2022/ Accepted: 25 July 2022/ Published: September 2022

Abstract: *This paper deals with the development of a novel time-domain analytical method to perform an aeroelastic stability analysis of a high aspect ratio wing. The aerodynamic model in this paper is built upon the frequency domain of Theodorsen aerodynamics. An inverse Fourier transform technique is applied to convert the Theodorsen frequency domain transfer function to the Wagner time-domain response function. Later, lift and moment expressions, containing aerodynamic lag states are obtained using the indicial function approach which performs the convolution of the unit step response Wagner lift function with arbitrary input and its time derivative using the principle of superposition. Additional equations containing the derivative of aerodynamic lag states are coupled with previously obtained lift and moment expressions to fully get the complete unsteady aerodynamic model in the time-domain. This time-domain unsteady aerodynamic model is then coupled with a combined bending torsion beam finite element model, using the state space approach. A complex eigenvalue analysis of this state space system is performed, using MATLAB, to determine both the static and dynamic aeroelastic stability boundary. Finally, in this paper, aeroelastic stability analysis of the high aspect ratio wing is performed using the current method and results are validated with MSC Nastran aeroelastic analysis and those available in the literature.*

Key Words: *Flutter, Divergence, Indicial function, Aerodynamic lag states, Eigen value analysis*

1. INTRODUCTION

High Altitude, Long Endurance HALE aircraft is characterized by wings with very high aspect ratios, which have the advantage of reducing the induced drag, thus leading to higher lift-to-drag ratios [1]. These characteristics make HALE aircraft achieve longer endurance, long-range, lower fuel consumption, and lesser environmental emissions. Besides, several advantages, large deformations and deflections associated with high aspect ratio wings make them vulnerable to destructive fluid-structure interactions and give rise to various aeroelastic instability problems, such as torsional divergence and flutter [2]. In literature, several aeroelastic studies are available. Van Schoor and Von Flotow [3], were the first who studied the aeroelasticity of high aspect ratio wings and demonstrated the effects of wing flexibility on the aeroelastic characteristics of the high aspect ratio wings. Later, Patil and Hodges [4], contributed toward the non-linear aeroelasticity of HALE aircraft and highlighted that they can be highly flexible even at low aerodynamic loading and encounter large deformations which affect modal characteristics and thus produce noticeable changes in aeroelastic behavior

of the high aspect ratio wings. Aeroelastic phenomena involves the interaction between the structure and aerodynamics. Aerodynamics is generally divided into steady, quasi-steady and unsteady models. Unsteady aerodynamic flows are most general time dependent flows, whereas steady and quasi-steady aerodynamic flows are derived from unsteady aerodynamic flows. Steady aerodynamics originates from ignoring all time dependencies in unsteady flows. Quasi-steady aerodynamic flow takes time dependency into account yet not fully unsteady as there is no lag between the angle of attack and response of the structure, as all pressure fluctuations over the wing and wake are instant because of low-frequency motion. Thus, steady, and quasi-steady models are not suitable for aeroelastic analysis as they fail to capture wake-associated lag effects encountered in subsonic unsteady aerodynamic flows. Haddadpour [5] demonstrated that quasi-steady aerodynamics yields inaccurate results for aeroelastic stability analysis. In literature, various unsteady aerodynamic models are used for aeroelastic analysis. Kier [6] compared the unsteady aerodynamic models such as Vortex Lattice Method (VLM) [7] , Doublet Lattice Method (DLM) [8] and extended strip theory and declared the last one as the most suitable for aeroelastic analysis due to ease of modelling and fast simulation times. However, the unsteady strip theory presented by Theodorsen [9] , widely used for aeroelastic analysis, is in frequency domain which represents the lift and pitching moment for a thin airfoil undergoing small harmonic oscillations in an incompressible flow. This frequency domain strip theory needs to be converted into time-domain which can then be appended with the structural dynamic model using state space system and achieve the advantages of fast and robust aeroelastic analysis in initial aircraft design phase. In this paper, an unsteady aerodynamic model, fully in the time-domain is developed using a novel approach of Indicial functions and aerodynamic lag states. This paper builds on the frequency domain Theodorsen unsteady aerodynamic model. The Wagner function [10] is used for the conversion of the Theodorsen function to its time equivalent using Inverse Fourier transform [11]. Later, a convolution approach [12] is used, where convolution of unit step response function with an arbitrary input and its time derivative is performed. Circulatory lift function containing convolution integral is then solved using differential equations. Additionally, a unique method which introduces aerodynamic lag states, which are result of integral of exponential functions is used. Finally, additional equations in the form of aerodynamic lag state derivatives are obtained using Leibniz integration rule [13], to solve for the unsteady lift and moment expressions fully in time-domain. This fully unsteady aerodynamic model is then coupled with the combined bending torsion Euler-Bernoulli beam finite element model for the development of aeroelastic stability analysis method fully in time-domain. Linear time invariant LTI State space system [14] is used to setup complete aeroelastic system in the MATLAB. After the development of method, an aeroelastic stability analysis of high aspect ratio wing is performed using a complex Eigen value analysis of state space system at different flight speeds. Lastly, the results are validated with literature and by performing complete aeroelastic stability analysis in MSC Nastran.

2. DEVELOPMENT OF NOVEL TIME-DOMAIN AERODYNAMIC MODEL

Theodorsen aerodynamic model deals with the unsteadiness associated with wake in the subsonic in-compressible flow. When a wing is pitching and heaving, vortices are shed from the trailing edge of airfoil and are propagated in the wake. This shed vorticity creates a pressure fluctuation, which propagates with the speed of sound causing some pressure information to propagate upstream in subsonic flow, making it difficult to model than supersonic flow, where all pressure information propagates downstream. In unsteady aerodynamics, lift exhibits a lag

with respect to input and will built up over time. Theodorsen [9] investigated these wake lag effects and called the forces that are caused by the wake vorticity or circulation as circulatory forces, whereas, the forces and moments that are caused by the flow potential, on the airfoil itself, as non-circulatory forces. Thodorsen function *C(k)* is a complex function, shown in Eq. (1), written in terms of reduced frequency $k = \frac{\omega b}{U}$, where ω shows the frequency of the structure. This function causes a lag in magnitude and phase difference between aerodynamic forces and structural degrees of freedom.

$$C(k) = F(k) + iG(k) \tag{1}$$

Total unsteady aerodynamic lift L and moment expressions M , consists of two parts, namely, circulatory such as L_C, M_C and non-circulatory lift such as L_{NC} and M_{NC}, as shown in Eq. (2). The aerodynamic model formulated in this paper has no flap control surface. Wing is exposed to general excitation due to heave h and pitch θ. Here, vertical direction is defined positive upwards. Therefore, lift and the vertical displacement h are positive upwards. Free stream velocity, elastic pitch angle, air density and effective angle of attack are represented by U, θ, ρ and α, respectively. The half chord and distance between mid of airfoil to elastic axis is shown by b and a, respectively.

$$\begin{gathered}
L = \rho b^2\left(U\pi\dot{\theta} + \pi\ddot{h} - \pi ba\ddot{\theta}\right) + 2\pi\rho UbC(k)\left(U\theta - \dot{h} + b\left(\frac{1}{2} - a\right)\dot{\theta}\right) \\
L_{NC} = \rho b^2\left(U\pi\dot{\theta} + \pi\ddot{h} - \pi ba\ddot{\theta}\right) \\
L_C = 2\pi\rho UbC(k)\left(U\theta - \dot{h} + b\left(\frac{1}{2} - a\right)\dot{\theta}\right) \\
\alpha = -\frac{\dot{h}}{U} + \theta + \frac{\dot{\theta}}{U}b\left(\frac{1}{2} - a\right) \\
M = -\rho b^2\left(U\pi\left(\frac{1}{2} - a\right)b\dot{\theta} + \pi b^2\left(\frac{1}{8} + a^2\right)\ddot{\theta} - \pi ba\ddot{h}\right) + M_C \\
M_{NC} = -\rho b^2\left(U\pi\left(\frac{1}{2} - a\right)b\dot{\theta} + \pi b^2\left(\frac{1}{8} + a^2\right)\ddot{\theta} - \pi ba\ddot{h}\right) \\
M_C = L_C.b(1/2 + a)
\end{gathered} \tag{2}$$

Circulatory parts are proportional to reduced frequency k, thus frequency dependent, whereas non-circulatory parts are independent of frequency. Hence, only circulatory parts of lift and moment expressions will be converted into time-domain. Dowell [11] and Garrick [15] demonstrated the equivalence of Theodorsen frequency domain transfer function and Wagner time-domain response function using Fourier transform method. The Theodorsen and Wagner functions are equivalent representations of the effect of wake in the frequency domain and time-domain, respectively. Inverse Fourier transform is applied to Theodorsen function as shown in Eq. (3).

$$\begin{gathered}
L_c(k) = 2\pi\rho U^2 b\alpha C(k) \\
L_c(t) = 2\pi\rho U^2 b\int_0^\infty \frac{\widehat{\alpha}}{ik}C(k)e^{ikt^*}dk \\
\int_0^\infty \frac{\widehat{\alpha}}{ik}C(k)e^{ikt^*}dk = \alpha\varphi(t^*) \\
L_c(t) = 2\pi\rho U^2 b\alpha\varphi(t^*)
\end{gathered} \tag{3}$$

Circulatory lift in frequency domain $L_c(k)$ is transformed into time-domain $L_c(t)$ using Wagner function $\varphi(t^*)$ [10] , a time dependent function, which shows circulatory lift built up over time due to a sudden step in angle of attack α. The step in angle of attack is replaced by its Fourier equivalent. $\varphi(t^*)$ is written in terms of non-dimensional time t^*, which is defined as number of half chord aircraft flown since the step-in angle of attack is applied.

$$\varphi(t^*) = 1 - \psi_1 e^{\frac{-\varepsilon_1(t^*)U}{b}} - \psi_2 e^{\frac{-\varepsilon_2(t^*)U}{b}}$$
$$\varphi(t^*) = 1 - 0.165e^{-0.0455(t^*)} - 0.335e^{-0.300(t^*)} \tag{4}$$

An approximate expression for Wagner function is given by Jones [16], given in Eq.(4). Poles of Theodorsen function, such as ε_1, ε_2 and curve fitting coefficients such as ψ_1, ψ_2 are obtained from Rational function approximation of Theodorsen function.

The convolution of the unit step response function with arbitrary input α and its time derivative defines the Indicial function approach [12]. This function describes the time dependency of the aerodynamic lift. The Indicial function is obtained by applying the convolution integral as in Eq. (5).

$$L_c = \int_0^t L_c\,(t)^{us}(t-\tau)\frac{d\alpha}{d\tau}d\tau$$
$$L_c(t)^{us} = 2\pi\rho U^2 b\varphi(t^*)1 \tag{5}$$

$L_c(t)^{us}$ is obtained by applying a unit step to amplitude in α. The step response function can be used to calculate response to arbitrary non-harmonic input using convolution. Using principle of superposition L_c can be written as shown in Eq. (6).

$$L_c = 2\pi\rho U^2 b(\alpha(0)\varphi(t) + \int_0^t \varphi(t-\tau)\frac{d\alpha}{d\tau}d\tau$$
$$\varphi(t-\tau) = 1 - \psi_1 e^{\frac{-\varepsilon_1(t-\tau)U}{b}} - \psi_2 e^{\frac{-\varepsilon_2(t-\tau)U}{b}} \tag{6}$$

The expression for α, from Eq. (2), contains first order derivatives of h and θ thus, time derivative of α, will lead to second order derivative of h and θ. Therefore, the partial Integration is used to lower the order of derivative to first order as given in Eq. (7).

$$L_c = 2\pi\rho U^2 b(\alpha(t)\varphi(0) - \int_0^t \frac{d\varphi(t-\tau)}{d\tau}\alpha(\tau)\,d\tau \tag{7}$$

$$\frac{d\varphi(t-\tau)}{d\tau} = -\psi_1\varepsilon_1\frac{U}{b}e^{-\frac{\varepsilon_1(t-\tau)U}{b}} - \psi_2\varepsilon_2\frac{U}{b}e^{-\frac{\varepsilon_2(t-\tau)U}{b}} \tag{8}$$

where, $\varphi(0) = 1 - \psi_1 - \psi_2$. Substituting expressions from Eq. (8) and α in Eq. (7), we get

$$L_c = 2\pi\rho U^2 b(\alpha(t)\varphi(0) + \int_0^t \left(\psi_1\varepsilon_1\frac{U}{b}e^{-\frac{\varepsilon_1(t-\tau)U}{b}} + \psi_2\varepsilon_2\frac{U}{b}e^{-\frac{\varepsilon_2(t-\tau)U}{b}}\right)\left(-\frac{\dot{h}}{U} + \theta + \frac{\dot{\theta}}{U}b\left(\frac{1}{2} - a\right)\right)d\tau) \tag{9}$$

Now each part of Eq. (9) will be evaluated. Partial Integration is successively used to lower the order of differential equations.

Evaluating terms related to $\dot{h}$, θ and $\dot{\theta}$ from Eq. (9) we get Eq. (10), Eq. (11) and Eq. (12), respectively.

$$\begin{aligned}
&\int_0^t \left(\psi_1\varepsilon_1\frac{U}{b}e^{-\frac{\varepsilon_1(t-\tau)U}{b}}\right)\left(-\frac{\dot{h}}{U}\right)d\tau = -\frac{\psi_1\varepsilon_1}{b}\left(h-\varepsilon_1\frac{U}{b}\int_0^t e^{-\frac{\varepsilon_1(t-\tau)U}{b}}hd\tau\right)\\
&\int_0^t \left(\psi_1\varepsilon_1\frac{U}{b}e^{-\frac{\varepsilon_1(t-\tau)U}{b}}\right)\left(-\frac{\dot{h}}{U}\right)d\tau = -\frac{\psi_1\varepsilon_1}{b}(h-\varepsilon_1\frac{U}{b}w_1)\\
&\int_0^t \left(\psi_2\varepsilon_2\frac{U}{b}e^{-\frac{\varepsilon_2(t-\tau)U}{b}}\right)\left(-\frac{\dot{h}}{U}\right)d\tau = -\frac{\psi_2\varepsilon_2}{b}\left(h-\varepsilon_2\frac{U}{b}\int_0^t e^{-\frac{\varepsilon_2(t-\tau)U}{b}}hd\tau\right)\\
&\int_0^t \left(\psi_2\varepsilon_{21}\frac{U}{b}e^{-\frac{\varepsilon_2(t-\tau)U}{b}}\right)\left(-\frac{\dot{h}}{U}\right)d\tau = -\frac{\psi_2\varepsilon_2}{b}(h-\varepsilon_2\frac{U}{b}w_2)
\end{aligned} \tag{10}$$

$$\begin{aligned}
&\int_0^t \left(\psi_1\varepsilon_1\frac{U}{b}e^{-\frac{\varepsilon_1(t-\tau)U}{b}}\right)\theta d\tau = \left(\psi_1\varepsilon_1\frac{U}{b}\right)\int_0^t \frac{U}{b}e^{-\frac{\varepsilon_1(t-\tau)U}{b}}\theta d\tau\\
&\int_0^t \left(\psi_1\varepsilon_1\frac{U}{b}e^{-\frac{\varepsilon_1(t-\tau)U}{b}}\right)\theta d\tau = \left(\psi_1\varepsilon_1\frac{U}{b}\right)w_3\\
&\int_0^t \left(\psi_2\varepsilon_2\frac{U}{b}e^{-\frac{\varepsilon_2(t-\tau)U}{b}}\right)\theta d\tau = \left(\psi_2\varepsilon_2\frac{U}{b}\right)\int_0^t \frac{U}{b}e^{-\frac{\varepsilon_2(t-\tau)U}{b}}\theta d\tau\\
&\int_0^t \left(\psi_2\varepsilon_2\frac{U}{b}e^{-\frac{\varepsilon_2(t-\tau)U}{b}}\right)\theta d\tau = \left(\psi_2\varepsilon_2\frac{U}{b}\right)w_4
\end{aligned} \tag{11}$$

$$\begin{aligned}
&\int_0^t \left(\psi_1\varepsilon_1\frac{U}{b}e^{-\frac{\varepsilon_1(t-\tau)U}{b}}\right)\left(\frac{\dot{\theta}}{U}b\left(\frac{1}{2}-a\right)\right)d\tau = \left(\psi_1\varepsilon_1\right)\left(\frac{1}{2}-a\right)\int_0^t e^{-\frac{\varepsilon_1(t-\tau)U}{b}}(\dot{\theta})d\tau\\
&\int_0^t \left(\psi_1\varepsilon_1\frac{U}{b}e^{-\frac{\varepsilon_1(t-\tau)U}{b}}\right)\left(\frac{\dot{\theta}}{U}b\left(\frac{1}{2}-a\right)\right)d\tau = \left(\psi_1\varepsilon_1\right)\left(\frac{1}{2}-a\right)(\theta-\varepsilon_1\frac{U}{b}(\int_0^t e^{-\frac{\varepsilon_1(t-\tau)U}{b}}\dot{\theta})d\tau\\
&\int_0^t \left(\psi_1\varepsilon_1\frac{U}{b}e^{-\frac{\varepsilon_1(t-\tau)U}{b}}\right)\left(\frac{\dot{\theta}}{U}b\left(\frac{1}{2}-a\right)\right)d\tau = \left(\psi_1\varepsilon_1\right)\left(\frac{1}{2}-a\right)\left(\theta-\varepsilon_1\frac{U}{b}w_3\right)\\
&\int_0^t \left(\psi_2\varepsilon_2\frac{U}{b}e^{-\frac{\varepsilon_2(t-\tau)U}{b}}\right)\left(\frac{\dot{\theta}}{U}b\left(\frac{1}{2}-a\right)\right)d\tau = \left(\psi_2\varepsilon_2\right)\left(\frac{1}{2}-a\right)\left(\theta-\varepsilon_2\frac{U}{b}w_4\right)
\end{aligned} \tag{12}$$

The lag effects of wake, that are present in the unsteady aerodynamics through the Theodorsen function, are represented in time-domain by aerodynamic lag states, w_1 to w_4 which increases the total number of states of system [17] and [18].

$$w_1 = \int_0^t e^{-\frac{\varepsilon_1(t-\tau)U}{b}} h d\tau; w_2 = \int_0^t e^{-\frac{\varepsilon_2(t-\tau)U}{b}} h d\tau$$
$$w_3 = \int_0^t e^{-\frac{\varepsilon_1(t-\tau)U}{b}} \theta d\tau; w_4 = \int_0^t e^{-\frac{\varepsilon_2(t-\tau)U}{b}} \theta d\tau \quad (13)$$

Now putting all the evaluated terms back into Eq. (9), we get the lift and moment expressions.

$$\begin{aligned} L_C = 2\pi\rho U^2 b \Bigg(& \alpha(t)\varphi(0) - \frac{\psi_1\varepsilon_1}{b}\left(h - \varepsilon_1\frac{U}{b}w_1\right) - \frac{\psi_2\varepsilon_2}{b}\left(h - \varepsilon_2\frac{U}{b}w_2\right) + \psi_1\varepsilon_1\frac{U}{b}w_3 \\ & + \psi_2\varepsilon_2\frac{U}{b}w_4 + (\psi_1\varepsilon_1)\left(\frac{1}{2} - a\right)\left(\theta - \varepsilon_1\frac{U}{b}w_3\right) \\ & + (\psi_2\varepsilon_2)\left(\frac{1}{2} - a\right)\left(\theta - \varepsilon_2\frac{U}{b}w_4\right)\Bigg) \end{aligned} \quad (14)$$
$$M_C = L_C b(1/2 + a)$$

Adding aerodynamic states to the governing aerodynamic equations, renders the system of equations non-solvable.

We have two expressions such as L_c and M_c from Eq.(14), but six unknowns such as h, θ, w_1, w_2, w_3 and w_4, so to make system solvable we need four more equations in the form of derivatives of aerodynamic lag states, which will now be derived using Leibniz Integration rule [13] as given below.

$$f(t) = \int_0^t e^{-\frac{\varepsilon_1(t-\tau)U}{b}} h(\tau) d\tau$$
$$\frac{df(t)}{dt} = g(t)\frac{d(t)}{dt} - g(0)\frac{d(0)}{dt} + \int_0^t \frac{d(e^{-\frac{\varepsilon_1(t-\tau)U}{b}} h(\tau))}{dt} d\tau \quad (15)$$

$$\dot{w_1} = h(t) - \frac{\varepsilon_1 U}{b}w_1, \dot{w_2} = h(t) - \frac{\varepsilon_2 U}{b}w_2$$
$$\dot{w_3} = \theta(t) - \frac{\varepsilon_1 U}{b}w_3, \dot{w_4} = \theta(t) - \frac{\varepsilon_2 U}{b}w_4 \quad (16)$$

Now the lift and moment expressions from Eq. (14), can be augmented with expressions from Eq.(16) , to get final lift and moment expressions fully in time-domain in Eq. (17) and Eq. (18) , respectively.

Here, S denote the depth of each node of FE model.

$$\begin{aligned} L = \rho b^2 S\left(U\pi\dot{\theta} + \pi\ddot{h} - \pi b a\ddot{\theta}\right) + 2\pi\rho U^2 b(\alpha(t)\varphi(0) - \frac{\psi_1\varepsilon_1}{b}(h - \varepsilon_1\frac{U}{b}w_1) - \\ \frac{\psi_2\varepsilon_2}{b}\left(h - \varepsilon_2\frac{U}{b}w_2\right) + \psi_1\varepsilon_1\frac{U}{b}w_3 + \psi_2\varepsilon_2\frac{U}{b}w_4 + \\ (\psi_1\varepsilon_1)(1/2 - a)(\theta - \varepsilon_1\frac{U}{b}w_3) + (\psi_2\varepsilon_2)(1/2 - a)(\theta - \varepsilon_2\frac{U}{b}w_4)) \end{aligned} \quad (17)$$

$$M = -\rho b^2 S\left(U\pi\left(\frac{1}{2}-a\right)b\dot{\theta} + \pi b^2\left(\frac{1}{8}+a^2\right)\ddot{\theta} - \pi b a\ddot{h}\right) + 2\pi\rho U^2 b^2\left(\frac{1}{2}+a\right)$$
$$(\alpha(t)\varphi(0) - \frac{\psi_1\varepsilon_1}{b}(h - \varepsilon_1\frac{U}{b}w_1) - \frac{\psi_2\varepsilon_2}{b}(h - \varepsilon_2\frac{U}{b}w_2) + \psi_1\varepsilon_1\frac{U}{b}w_3 + \psi_2\varepsilon_2\frac{U}{b}w_4 + \quad (18)$$
$$(\psi_1\varepsilon_1)(1/2-a)(\theta - \varepsilon_1\frac{U}{b}w_3) + (\psi_2\varepsilon_2)(1/2-a)(\theta - \varepsilon_2\frac{U}{b}w_4))$$

3. DEVELOPMENT OF STRUCTURAL MODEL

The Ritz method [19], is used for finite element formulation presented in this paper, which calculates approximate solution to a differential equation subjected to a set of boundary conditions. The solution function of a differential equation is assumed to be a linear combination of shape functions each having a different weight. The finite element method describes the displacement field of small portion, called an element using a shape function. A beam model based on Euler Bernoulli beam theory is used in this paper ;it has three degrees of freedom [20], where, two degrees of freedoms related to bending, $x_B = [h_i\ \phi_i]^t$, such as, heave displacement h and an out-of-plane bending rotation φ and one degree of freedom related to torsion $x_T = [\ \theta_i]^t$, at each node. The shape functions for the Euler-Bernoulli beam have to be C1-continuous for which Hermitian shape functions are used. δ and ζ are shape functions related to h and φ, respectively, whereas, γ shows θ related shape function. These shape functions have to be consistent with the geometric boundary conditions. For 2 node beam element shape functions are shown in Eq. (19).

$$\delta_1 = \frac{1}{4}(2-\frac{2y}{L})^2(1+\frac{2y}{L});\ \delta_2 = \frac{1}{4}(\frac{2y}{L})^2(3-\frac{2y}{L})$$
$$\zeta_1 = \frac{L}{8}(2-\frac{2y}{L})^2(\frac{2y}{L});\ \zeta_2 = \frac{L}{8}(\frac{2y}{L})^2(\frac{2y}{L}-2) \quad (19)$$
$$\gamma_1 = 1-\frac{1}{2}(\frac{2y}{L});\ \gamma_2 = \frac{1}{2}(\frac{2y}{L})$$

$S_B = [\delta_i\ \zeta_i]$ and $S_T = [\gamma_i]$, show shape function matrices. Displacement field of complete structure is discretized to an individual element. $x_T(y) = x_T S_T$ and $x_B(y) = x_B S_B$. Kinetic and potential energy terms are given in [19], where, $\dot{x_B} = \frac{d}{dt}(x_B)$ and $S_B{}'' = \frac{d^2(S_B)}{d^2y}$. S_B shows the curvature of beam, which is a second spatial derivative of bending shape functions. A uniform beam element is considered, where, *L, EI, GJ, m* and I_θ shows, length, flexural rigidity, torsional rigidity, mass per unit length and moment of inertia for twist per unit length. Finally, by the application of Lagrange method, stiffness and mass matrices are calculated. The spatial derivatives are transformed from global coordinate *y* to a non-dimensional local coordinate η which is defined from -1 to 1. The integration is carried out on the integrals ranging from -1 to 1 instead of 0 to *L* which is total length of beam.

$$K_B = \frac{8EI}{L^3}\int_{-1}^{1} B_B{}'' B_B{}''^t d\eta;\ M_B = \frac{mL}{2}\int_{-1}^{1} B_B{}^t B_B d\eta$$
$$K_T = \frac{2GJ}{L}\int_{-1}^{1} B_T{}' B_T{}'^t d\eta;\ M_T = \frac{I_\theta L}{2}\int_{-1}^{1} B_T B_T{}^t d\eta \quad (20)$$
$$K_{BT} = \frac{C}{L}\int_{-1}^{1} B_B{}''^t B_T{}' d\eta;\ M_{BT} = \frac{mLbx_\theta}{2}\int_{-1}^{1} B_B{}^t B_T d\eta$$

B_B shows the shape function, transformed from global coordinate to local coordinate represented in terms of $\eta = \frac{2y}{L} - 1$. $B_B{}'' = \frac{d^2}{d\eta^2}(B_B)$. The coupling stiffness and mass matrix are shown below, where C shows the coupling factor [20]. Coupling will be present, if the centre of gravity axis and elastic axis does not coincide with each other. Distance between elastic axis and CG axis non dimensional with half chord b is shown by bx_θ.

$$K_s = \begin{bmatrix} K_B & K_{BT} \\ K_{BT}{}^T & K^T \end{bmatrix}; M_s = \begin{bmatrix} M_B & M_{BT} \\ M_{BT}{}^T & M^T \end{bmatrix} \tag{21}$$

4 ANALYSIS

The most general form of aeroelastic governing equations is given below,

$$\begin{gathered} M_s\ddot{x} + K_s x = P_a \\ M_s\ddot{x} + K_s x = \begin{bmatrix} L \\ 0 \\ M \end{bmatrix} \end{gathered} \tag{22}$$

where, x, shows the displacement degrees of freedom. P_a shows the external aerodynamic forces which are acting on structure and consists of lift force L and a moment around elastic axis M. M_s and K_s shows the global structural mass and stiffness matrices, respectively.
Lift is associated with out of plane displacement h and will also take care of total bending rotation φ, but the bending itself will not be covered by bending loads due to aerodynamics. Moment around the elastic axis is associated with torsional rotation θ. Putting the Lift and moment expressions from Eq. (17) and Eq. (18), into Eq. (22) we get.

$$M_s\ddot{x} + K_s x = M_a\ddot{x} + C_a\dot{x} + K_a x + W x_a \tag{23}$$

where, M_a, K_a and C_a shows the aerodynamic mass, stiffness, and damping matrices, respectively. W shows the aerodynamic lag states matrix and x_a shows the aerodynamic lag states degrees of freedom. Separating the relevant terms from the lift and moment expressions we get aerodynamic matrices as shown below.

$$M_a = \begin{bmatrix} \rho b^2 S\pi & 0 & -\rho b^3 S\pi a \\ 0 & 0 & 0 \\ \rho b^3 S\pi a & 0 & -\rho b^4 S\pi(\frac{1}{8} + a^2) \end{bmatrix} \tag{24}$$

$$C_a = \begin{bmatrix} -2\rho bUS\pi\varphi(0) & 0 & \rho b^2 SU\pi(1 + 2(\frac{1}{2} - a)\varphi(0)) \\ 0 & 0 & 0 \\ -2\rho b^2 US\pi(\frac{1}{2} + a)\varphi(0) & 0 & \rho b^3 US\pi(\frac{1}{2} - a)(-1 + 2(\frac{1}{2} + a)\varphi(0)) \end{bmatrix} \tag{25}$$

$$K_a = 2\rho U^2 S\pi(\psi_1\varepsilon_1 + \psi_2\varepsilon_2)\begin{bmatrix} -1 & 0 & \frac{b(\varphi(0) + (\psi_1\varepsilon_1 + \psi_2\varepsilon_2)(\frac{1}{2} - a))}{(\psi_1\varepsilon_1 + \psi_2\varepsilon_2)} \\ 0 & 0 & 0 \\ b(\frac{1}{2} + a) & 0 & \frac{b^2(\frac{1}{2} + a)(\varphi(0) + (\psi_1\varepsilon_1 + \psi_2\varepsilon_2)(\frac{1}{2} - a))}{(\psi_1\varepsilon_1 + \psi_2\varepsilon_2)} \end{bmatrix} \tag{26}$$

$$W = 2\pi\rho U^3(\frac{1}{2}+a)S\begin{bmatrix} \frac{\psi_1\varepsilon_1^2}{b(\frac{1}{2}+a)} & \frac{\psi_2\varepsilon_2^2}{b(\frac{1}{2}+a)} & \frac{\psi_1\varepsilon_1(1-\varepsilon_1(\frac{1}{2}-a))}{(\frac{1}{2}+a)} & \frac{\psi_2\varepsilon_2(1-\varepsilon_2(\frac{1}{2}-a))}{(\frac{1}{2}+a)} \\ 0 & 0 & 0 & 0 \\ \psi_1\varepsilon_1\varepsilon_1 & \psi_2\varepsilon_2\varepsilon_2 & \psi_1\varepsilon_1(1-\varepsilon_1(\frac{1}{2}-a))b & \psi_2\varepsilon_2(1-\varepsilon_2(\frac{1}{2}-a))b \end{bmatrix} \quad (27)$$

$$W_0 = \begin{bmatrix} -\frac{\varepsilon_1 U}{b} & 0 & 0 & 0 \\ 0 & -\frac{\varepsilon_2 U}{b} & 0 & 0 \\ 0 & 0 & -\frac{\varepsilon_3 U}{b} & 0 \\ 0 & 0 & 0 & -\frac{\varepsilon_4 U}{b} \end{bmatrix} \quad (28)$$

Aeroelastic mass and stiffness matrices M_{ae} and K_{ae} are shown in Eq. (29).

$$\begin{gathered} M_{ae}\ddot{x} - C_a\dot{x} - K_{ae}x + Wx_a \\ M_{ae} = M_s - M_a \\ K_{ae} = K_s - K_a \end{gathered} \quad (29)$$

General form of state space equation is presented in Eq. (30) given by Fortmann [21]. The state space technique uses the first order ordinary differential equations to describe the governing aeroelastic equation, which are of second order. A state space approach similar to Karpel [14] is used in this paper. X is states of the system and u is inputs to the system. For aeroelastic stability analysis inputs u do not affect the stability of the system.

$$\begin{gathered} \dot{X} = AX + Bu \\ \dot{X} = AX; X = \begin{bmatrix} \dot{x} \\ x \\ x_a \end{bmatrix} \end{gathered} \quad (30)$$

Writing the matrices in state space form we get the state space matrix A, given below.

$$A = \begin{bmatrix} {M_{ae}}^{-1}C_a & -{M_{ae}}^{-1}K_{ae} & {M_{ae}}^{-1}W \\ I & 0 & 0 \\ 0 & II & W_0 \end{bmatrix} \quad (31)$$

$$I = \begin{bmatrix} 1 & 0 & 0 \\ 0 & 1 & 0 \\ 0 & 0 & 1 \end{bmatrix}; II = \begin{bmatrix} 1 & 0 & 0 \\ 1 & 0 & 0 \\ 0 & 0 & 1 \\ 0 & 0 & 1 \end{bmatrix} \quad (32)$$

$$\begin{gathered} \lambda X = AX \\ (A - \lambda I)X = 0 \\ det[A - \lambda I] = 0 \end{gathered} \quad (33)$$

Aeroelastic stability analysis is basically a complex Eigen value analysis of the state space matrix A, which yields complex Eigen values, $\lambda = \sigma + i\omega$, where, damping σ and frequency ω, show real and imaginary parts, respectively.

Due to the fact that aerodynamic stiffness and damping matrices are dependent on airspeed, so to determine the aeroelastic instability, complex Eigen value analysis is needed to be performed over the range of different air speeds.
Aeroelastic system will be unstable when $\sigma > 0$. Additionally, $\omega \neq 0$ shows flutter while, $\omega = 0$ shows divergence.
Divergence can also be found out by performing real eigen value analysis of static aeroelastic equation given below.

$$(K_s - qK_a - \lambda)X = 0$$
$$det[K_s - qK_a - \lambda] = 0 \tag{34}$$

5. RESULTS AND VALIDATION

Aircraft model data are obtained from [4]. Material properties of wing are selected on hit and trial basis to get the desired modal frequencies of wing.
Eigen value analysis of structural mass and stiffness matrices is performed using MATLAB to compute normal modes of wing. The mode shapes of the first few modes are shown in Figure 1.

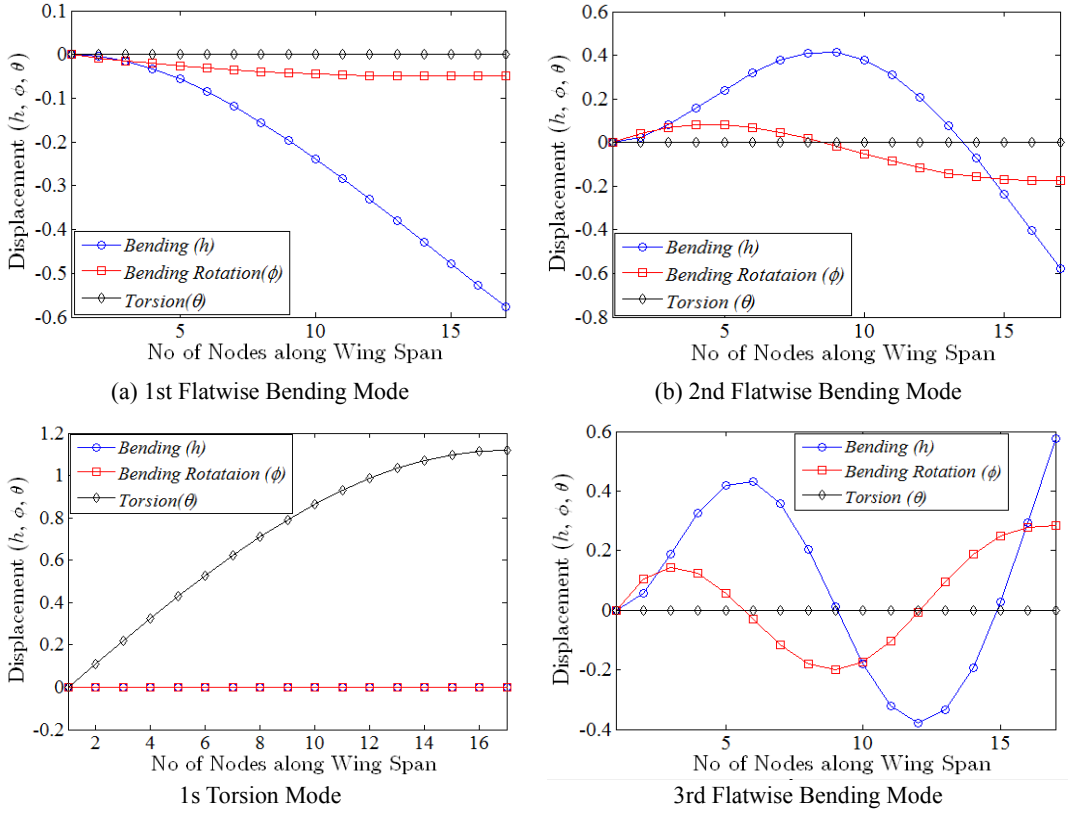

(a) 1st Flatwise Bending Mode

(b) 2nd Flatwise Bending Mode

1s Torsion Mode

3rd Flatwise Bending Mode

Figure 1. Normal Modes Analysis of Wing

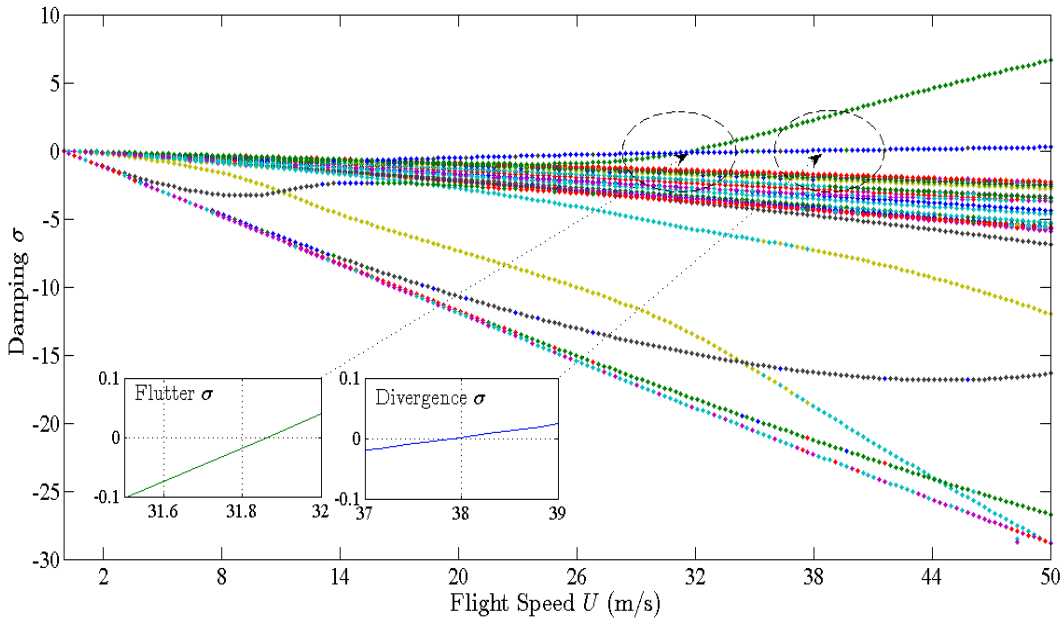

Figure 2. Flight Speed vs Damping

Flutter speed will be the lowest speed at which at least one Eigen value yields positive damping and non-zero frequency. From the Figure 2, it is seen that there are two curves crossing the zero-damping line. Flutter curve crosses the damping line at lower speed. Modes of the structure coalesce with each other to cause flutter instability at a certain frequency as shown in Figure 3. The lowest speed at which at least one Eigen value yields positive damping and zero frequency will give out divergence speed. Divergence corresponds to the zero frequency as shown in Figure 3. The divergence analysis is performed using two methods, firstly using the State Space Matrix A and secondly using the Static Aeroelastic equation Eq. (34).

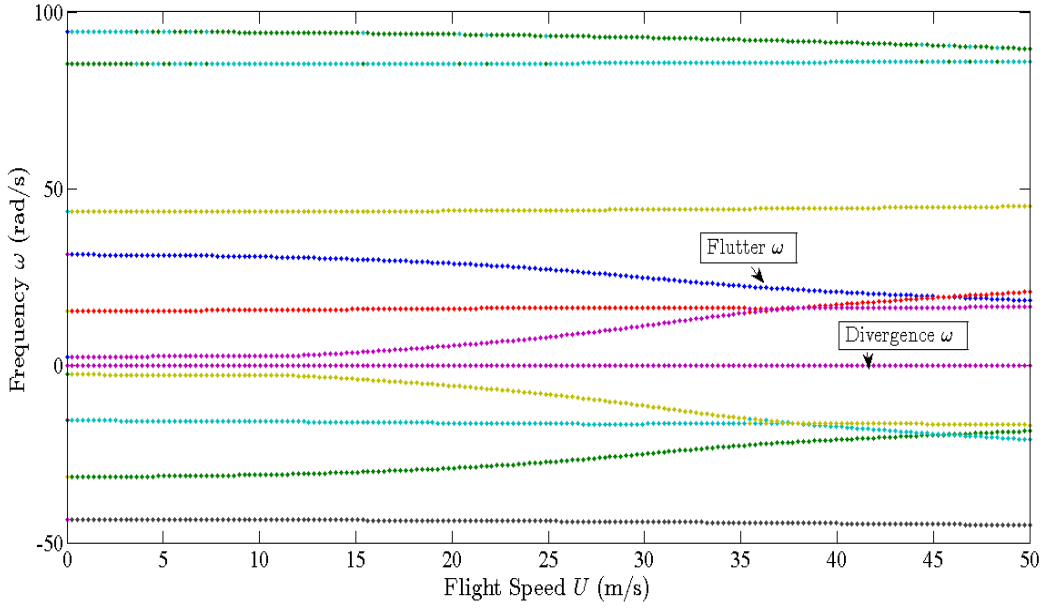

Figure 3. Flight Speed vs Frequency

The convergence of flutter and the divergence speed with increasing number of beam elements are shown below in Figure 4. It is seen that the flutter speed decreases rapidly as the number of beam elements increases but converges for about 16 beam elements. The divergence speed does not vary significantly with change in number of elements.

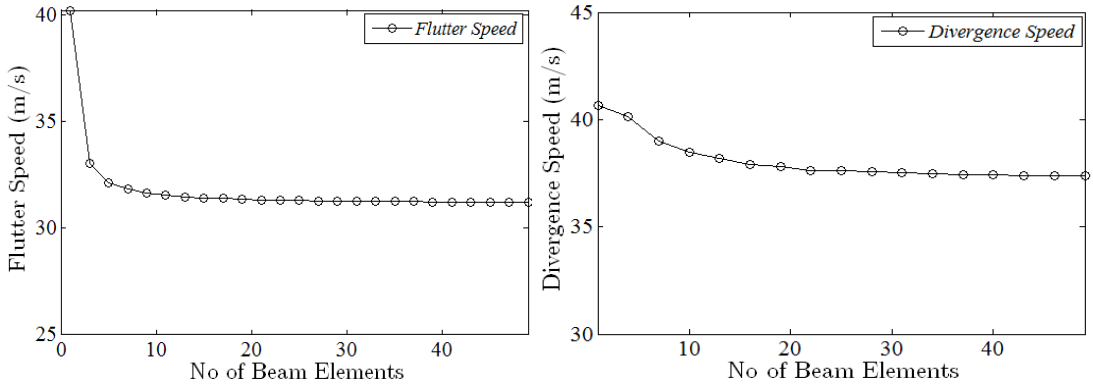

(a) Convergence of Flutter Speed (b) Convergence of Divergence Speed

Figure 4. Convergence of Flutter and Divergence speed with increasing number of beam elements

In aeroelasticity, the stiffness matrix is complex, so we get complex Eigen values and subsequently, complex Eigen modes. The Complex Eigen modes are different from the real modes. The Real modes are just a scaling of a certain shape of motion of wing. A complex mode has always to plot in time, as there is a phase shift between the motions of the different points along the wing, due to the presence of imaginary part. The complex flutter mode are plotted separately over the wing span in Figure 5.

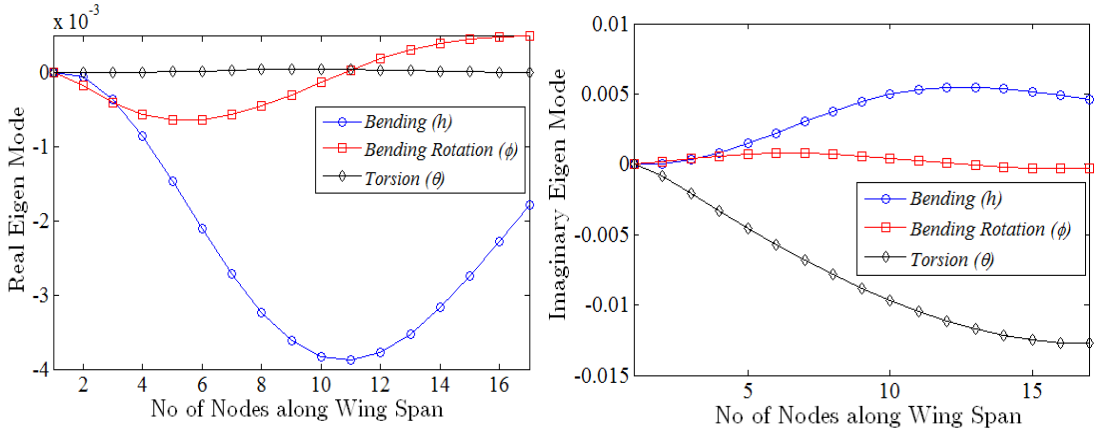

(a) Real Flutter Eigen Mode (b) Imaginary Flutter Eigen Mode

Figure 5. Complex Flutter Mode

MSC Nastran and Patran are used for structural and aerodynamic modelling and analysis. Wing structure is modeled using 16 CBEAM elements each of length of 1m as shown in Figure 6(a). Wing material properties are selected after reading several papers and properties of Elastic modulus E = 70 GPa and Poisons Ratio = 0.3 is used. Properties of beam elements are added using PBEAM card. The area moment of inertia I_{11} and I_{22} are obtained by dividing Span wise and Chord wise bending Rigidity by E elastic modulus value. The Torsional Constant is obtained by dividing Torsional rigidity by G modulus of rigidity value.

The Weight of structure is added using lumped masses using CONM2 point elements. The Mass per unit length is used to calculate the value of each point mass. CONM2 elements distance from the structural nodes are varied to get the Moment of inertia per unit length equal to 0.1 Kg.m and finally placed at ±0.371m of each of the 17 structural nodes.
The Structural nodes are connected to CONM2 elements using Rigid Bars RBE2. The Wing is modeled as cantilever beam, so Root node of Wing is constrained in all 6 Degree of freedoms. The Aerodynamic mesh of 32 span wise boxes and 10 chord wise boxes, as shown in Figure 6(b), is given by CAERO card.

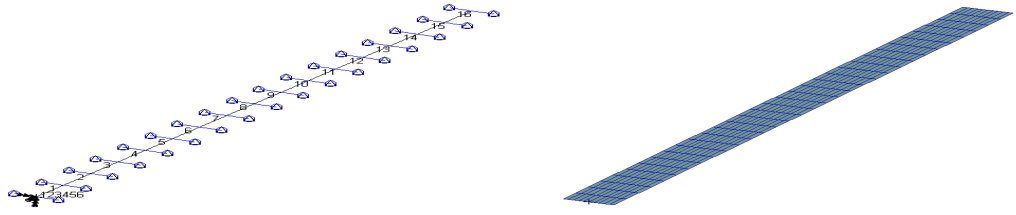

(a) Nastran Structural Model Wing (b) Nastran Aerodynamic Model Wing

Figure 6 . MSC Nastran Wing Model

MKAERO2 card defines the reduced frequency and Mach pairs. FLFACT card defines the velocity and density ratio. SPLINE5 is used for coupling of structural and aerodynamic model. EIGRL card is used to call Eigen value analysis, whereas FLUTTER card is used to call flutter analysis using MSC Nastran as solver. Nastran SOl 103 is used for modal analysis while SOl 145 is used for flutter analysis [22].

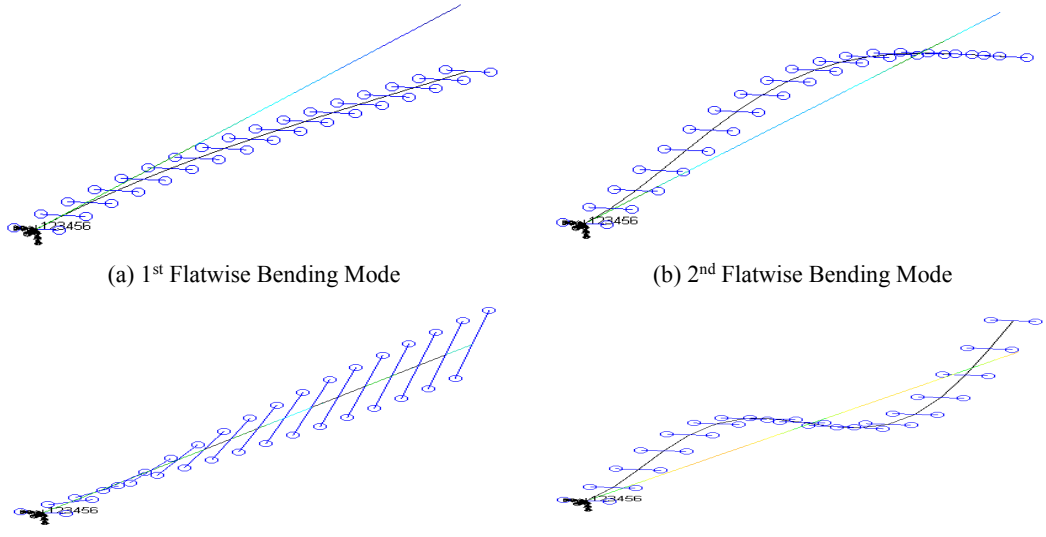

(a) 1st Flatwise Bending Mode (b) 2nd Flatwise Bending Mode

(c) 1st Torsion Mode (d) 3rd Flatwise Bending Mode

Figure 7. Normal Modes of Wing MSC Nastran

Modal analysis of wing is performed in MSC Nastran using SOL 103.Mode shapes of first few normal modes are shown in Figure 7. Nastran flutter summary is given in Figure 8 and Figure 9, respectively.
Table 1 and Table 2 show the modal analysis and aeroelastic analysis results performed using the current method and are found to be accurately validated with commercial software like MSC Nastran and analysis performed by Patil [4].

Table 1. Normal Modes Analysis Results and Validation

Mode Shape	Current Analysis	MSC Nastran Sol 103	Patil [4]
	Frequency(rad/s)		
1st Flatwise Wing Bending	2.243	2.232	2.247
2nd Flatwise Wing Bending	14.056	14.016	14.056
1st Wing Torsion	31.058	31.321	31.046
3rd Flatwise Wing Bending	39.358	39.315	39.356

Table 2. Aeroelastic Stability Analysis Results and Validation

Aeroelastic Stability Parameters	Current Analysis		MSC Nastran Sol 145	Patil [4]
	State Space Matrix *A*	Static Aeroelastic Equation		
Flutter Speed (m/s)	31.86		30.63	32.21
Flutter Frequency (rad/s)	23.97		24.52	22.61
Divergence Speed (m/s)	37.91	37.13	39.45	37.29

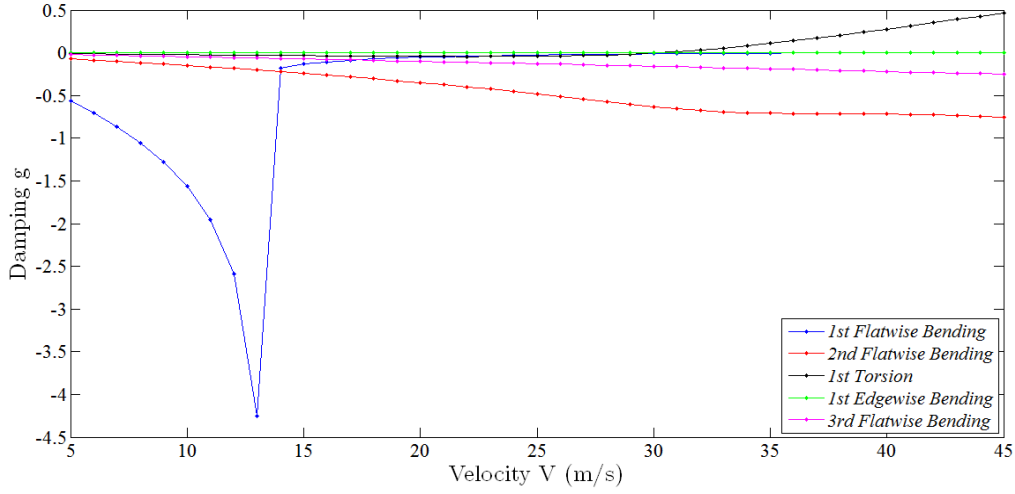

Figure 8. Nastran Flutter Summary: Flight Speed vs Damping

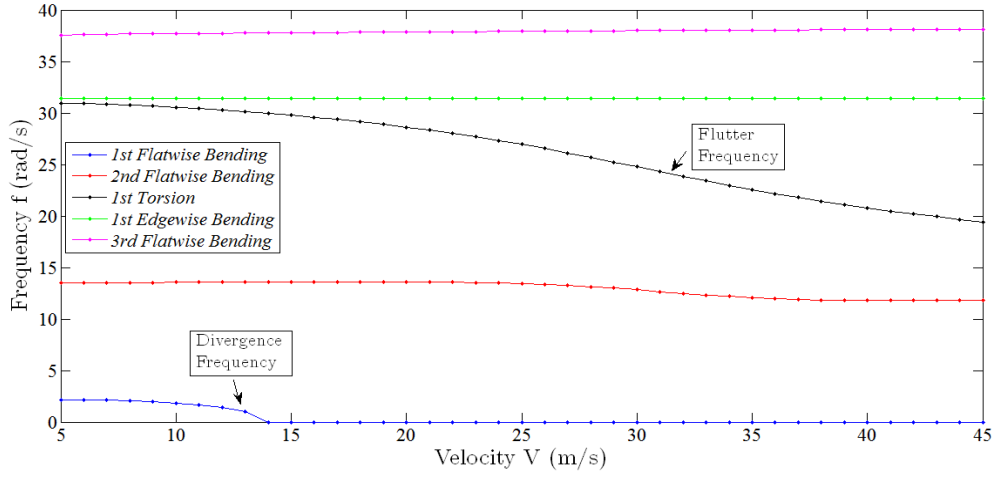

Figure 9. Nastran Flutter Summary: Flight Speed vs Frequency

6. CONCLUSIONS

The flutter and divergence characteristics of the wing are dependent on the complex Eigen modes of the wing. The structural modes of the wing coalesce with each other at a certain frequency and at a certain airspeed which cause an aeroelastic instability like flutter to occur. Low frequency modes of structure are more important for the aeroelastic instability. It is evident from analysis that the flutter aeroelastic instability is more critical as it occurs at low flight speed. The development of this method provides an accurate and time efficient method to compute the aeroelastic stability of high aspect ratio wing and can replace other methods like Doublet Lattice method and Computational fluid dynamics and commercial packages like MSC Nastran for the initial design phases of the wing.

REFERNCES

[1] I. H. Abbott and, A. V. Doenhoff, *Theory of wing sections, including a summary of airfoil data*, New York: Dover Publications, 1959.
[2] T. E. Noll, J. M. Brown and D. M. Perez, *Investigation of the Helios prototype aircraft mishap*, NASA, 2004.
[3] M. C. Van Schoor and A. H. Von Flotow, Aeroelastic Characteristics of a highly flexible Aircraft, *J. Aircr.,* vol. **27**, no. 10, pp. 901-908, 1990.
[4] M. J. Patil, D. H. Hodges and C. S. Cesnik, Nonlinear Aeroelasticity and Flight Dynamics of High-Altitude Long-Endurance Aircraft, *J. Aircr.,* vol. **38**, no. 1, pp. 88--94, 2001.
[5] H. Haddadpour and R. D. FirouzAbadi, Evaluation of quasi-steady aerodynamic modeling for flutter prediction of aircraft wings in incompressible flow, *Thin-Walled Struct.,* vol. **44**, no. 9, pp. 931-936, 2006.
[6] T. Kier, *Comparison of Unsteady Aerodynamic Modelling Methodologies with Respect to Flight Loads Analysis*, AIAA AFM Conference and Exhibit, San Francisco, California, 2005.
[7] J. Murua, R. Palacios and J. R. Graham, Applications of the unsteady vortex-lattice method in aircraft aeroelasticity and flight dynamics, *Prog. Aero. Sci.,* vol. **55**, pp. 46-72, 2012.
[8] E. Albano and W. P. Rodden, A doublet-lattice method for calculating lift distributions on oscillating surfaces in subsonic flows, *AIAA J.,* vol. **7**, no. 2, pp. 279--285, 1969.
[9] T. Theodorsen, *General theory of aerodynamic instability and the mechanism of futter*, NACA Report. 496, 1935.
[10] H. Wagner, Über die entstehung des dynamischen auftriebes von tragflügeln, *Appl. Math. Mech.,* vol. **5**, no. 1, pp. 17-35, 1925.
[11] E. H. Dowell, *A Simple Method for Converting Frequency Domain Aerodynamics into the Time-domain*, NASA. TM. 81844, 1980.
[12] Y. C. Fung, *An introduction to the theory of aeroelasticity*, New York: Dover Publications, 1993.
[13] G. Stephenson, *Mathematical methods for science students*, London: Longman Publishers, 2nd Edition, 1973.
[14] M. Karpel, Design for Active Flutter Suppression and Gust Alleviation Using State-Space Aeroelastic Modeling, *J. Aircr.,* vol. **19**, no. 3, pp. 221--227, 1982.
[15] I. E. Garrick, *On some reciprocal relations in the theory of nonstationary flows*, NACA Report. 629, 1938.
[16] R. T. Jones, *The Unsteady Lift of a Wing of Finite Aspect Ratio*, NACA Report. 681, 1940.
[17] J. W. Edwards, H. Ashley and J. V. Breakwell, Unsteady Aerodynamic Modeling for Arbitrary Motions, *AIAA.J,* vol. **17**, no. 4, pp. 365--374, 1979.
[18] M. H. Dinyavari and P. P. Friedmann, *Finite State Arbitrary Motion Aerodynamics to Rotor Blade Aeroelastic Response in Hover and Forward Flight*, AIAA/ASME/ASCE/AHS 26th Struct. Struct. Dyn. Mater. Conf., 1985.
[19] J. R. Wright and J. E. Cooper, *Introduction to Aircraft Aeroelasticity and Loads*, England: John Wiley Sons, Ltd, 2007.
[20] R. D. Breuker, S. Binder and A. Wildschek, *Combined Active and Passive Loads Alleviation through Aeroelastic Tailoring and Control Surface/Control System Optimization*, AIAA Aerosp. Sci. Meet. 8--12 January 2018, 2018.
[21] T. E. Fortmann and K. L. Hitz, *An Introduction to Linear Control Systems*, Marcel Dekker, Inc. New York and Basel, 1977.
[22] W. P. Rodden and E. H. Johnson, *MSC NASTRAN Aeroelastic analysis User's guide,* MSC. Version 68, 1994.